A NONLINEAR SIMULATION MODEL FOR ACTIVE MAGNETIC BEARING ACTUATORS

H. Springer,[1] G. Schlager,[2] T. Platter[3]

ABSTRACT

A magnetic network theory is presented to model the stator, rotor and airgap flux paths of active magnetic bearing actuators. Nonlinear empirical magnetization laws including hysteresis and saturation of the ferromagnetic core materials are employed. Open loop multidimensional state space equations for magnetic bearing actuators are carried out to determine the magnetic flux density to field strength trajectories within any path of the bearing network model. Nonlinear actuator airgap forces are calculated, and the governing dynamic equations of an active magnetic bearing are presented in a compact matrix form. A numerical example is employed for a closed loop voltage controlled system of a radial 8-pole bearing.

1 INTRODUCTION

If severe operating conditions occur to an active magnetic bearing (AMB) with high dynamic loads, then nonlinear saturation characteristics of the bearing actuators and power amplifiers may become effectiv. Nonlinear AMB-characteristics are represented, for example, by nonlinear airgap force to displacement relationships, nonlinear force to current relationships, nonlinear magnetization laws for the ferromagnetic core materials of stator and rotor including magnetic saturation and hysteresis effects, non-conservative magnetic cross-coupling forces due to eddy-current losses in the running rotor, saturation and switching effects of power amplifiers, and nonlinear sensor effects for large shaft displacements.

In this paper a nonlinear model is developed for radial-AMB actuators including nonlinear force to displacement and force to current relationships. Further, magnetic saturation and hysteresis of the ferromagnetic core material are taken into account. The magnetic properties of the stator material may also be anisotropic. The whole bearing actuator is modelled as a multi-node network of variable magnetic reluctances (including back-iron paths of the stator) located between the model node points, see (Maslen, Meeker, 1994), (Maslen, Meeker, 1995) and (Schmidt, Platter, Springer, 1996), for example. In the magnetic circuit model leakage and fringing effects are neglected as usual, and the flux density along a path between two node

[1]Vienna University of Technology, A-1040 Wien, Austria.
[2]SDP-AG, Technology Center, A-4400 Steyr, Austria.
[3]Siemens SGP Transportation Systems, A-1110 Wien, Austria.

points (pole legs, stator back-iron, rotor and airgaps) is assumed to be constant. However, the local magnetic permeability dB/dH of a one dimensional network path element may be a function of the preceding magnetization history of the core material including saturation effects also. In the current state of the model the theory does not yet consider reversing magnetization effects in the non-stationary path elements of a turning rotor. Ferromagnetic material equations including hysteresis have been developed by (Hodgdon, 1988a,b), and (Springer, Maslen, Humphris, 1990), for example. In this paper the empirical magnetization model of M. L. Hodgdon is introduced.

2 LIST OF NOMENCLATURE

The most important symbols used in this paper are listed below; see also Fig. 1, Fig. 2, Fig. 3 and the appendix.

$\mathbf{A}_{p,b,r}$	(n x n)-cross section matrix of the fluxes of p, b, r - path elements, resp.
$\mathbf{B}_{g,p,b,r}$	(n x 1)-flux density vector for g, p, b, r - path elements, resp.
$\mathbf{F}_{ex}(t)$	(2 x 1)-external force vector exerted to the rotor.
$\mathbf{g}(\mathbf{x})$	(n x n)-airgap lengths matrix depending on shaft displacements.
$\mathbf{H}_{g,p,b,r}$	(n x 1)-field strength vector for g, p, b, r - path elements, resp.
$\mathbf{I}(t)$	(n x 1)-coil current vector.
$\mathbf{I}_s(t)$	(m x 1)-source current vector.
$\mathbf{M}$	(2 x 2)-rotor mass matrix.
$\mathbf{n}$	(n x n)-number of turns matrix for the coils.
$\mathbf{r}_c$	(n x n)-coil resistance matrix.
$\mathbf{U}_A(t)$	(6n + m) x 1-actuator supply voltage vector.
$\mathbf{U}_B$	(k x 1)-biasing voltage vector.
$\mathbf{U}_C(t)$	(k x 1)-control voltage vector.
$\mathbf{U}_S(t)$	(m x 1)-supply voltage vector.
$\mathbf{V}$	(6n + m) x k-voltage distribution matrix.
$\mathbf{x}$	rotor (shaft) displacement vector $\mathbf{x} = [x, y]^T$
$\mathbf{Z}$	(6n + m) x 1-actuator state vector.
$\Phi_{g,p,b,r}$	(n x n)-flux vector for g, p, b, r - path elements, resp.
$\mu_{p,b,r}$	(n x n)-local permeability matrix for p,b,r-path elements, resp.
μ_0	magnetic permeability of free space.

3 MAGNETIC NETWORK THEORY

Figure 1 shows the magnetic network (paths and node points) for stator, rotor, and airgap of an n-pole radial AMB along with the coil locations. From Ampere's loop law for n closed loops of the stator network and one closed loop along the rotor circumference, the relations

$$\mathbf{e}^T\mathbf{g}(\mathbf{x})\mathbf{H}_g + \mathbf{e}^T\mathbf{p}\mathbf{H}_p + \mathbf{b}\mathbf{H}_b + \mathbf{r}\mathbf{H}_r = \mathbf{e}^T\mathbf{n}\mathbf{I}(t), \qquad (1)$$

$$\mathbf{S}^T\mathbf{r}\mathbf{H}_r = 0. \qquad (2)$$

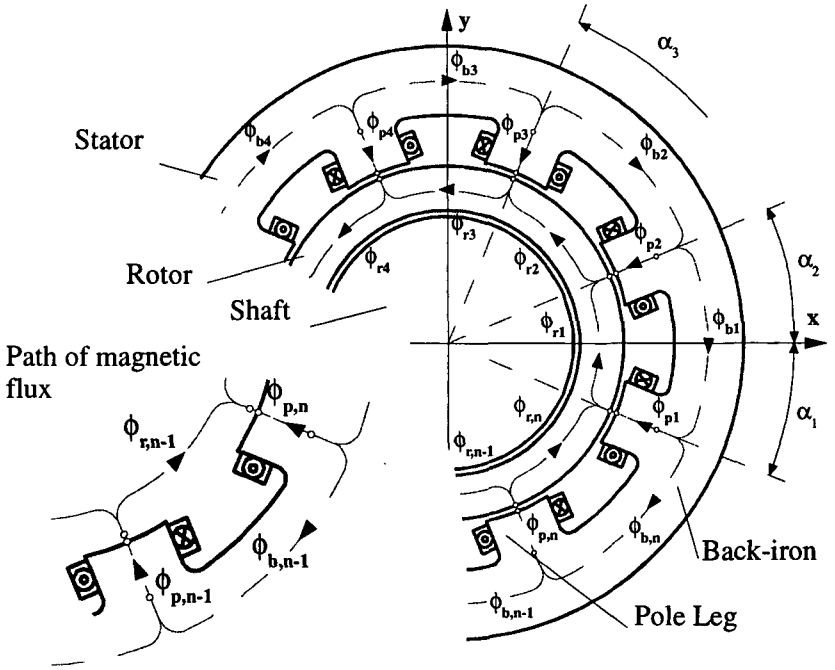

Figure 1. Magnetic network model for stator, rotor and airgaps

are obtained, where $\mathbf{g}(\mathbf{x}) = \mathbf{diag}[g_i(\mathbf{x})]$, $\mathbf{p} = \mathbf{diag}[p_i]$, $\mathbf{b} = \mathbf{diag}[b_i]$, $\mathbf{r} = \mathbf{diag}[r_i]$ are (n x n)-diagonal path lengths matrices for airgaps, poles, backiron, and rotor, respectively. $\mathbf{H_g} = \mathbf{col}\{H_{gi}\}$, $\mathbf{H_p} = \mathbf{col}\{H_{pi}\}$, $\mathbf{H_b} = \mathbf{col}\{H_{bi}\}$, $\mathbf{H_r} = \mathbf{col}\{H_{ri}\}$ are the corresponding (n x 1)-field strength vectors with i = 1, 2, ...n. $\mathbf{S} = \{1, ...1\}^T$ is a summation vector. The coil currents are represented by the (n x 1)-vector $\mathbf{I}(t) = \mathbf{col}\{I_i(t)\}$ with the corresponding (n x n)-diagonal turns matrix $\mathbf{n} = \mathbf{diag}[N_i]$. Note that the airgap lengths matrix $\mathbf{g}(\mathbf{x})$ depends on the rotor radial displacement vector $\mathbf{x} = [x,y]^T$ measured within the x-y-reference frame as shown in Fig.1.

From the magnetic flux continuity equations for n nodes of the stator network, (n - 1) nodes of the rotor network, and n airgaps, respectively, the relations

$$\mathbf{d}\Phi_p - \mathbf{e}\Phi_b = \mathbf{0}, \tag{3}$$

$$\mathbf{d}'\Phi_g - \mathbf{e}'\Phi_r = \mathbf{0}, \tag{4}$$

$$\Phi_g - \Phi_p = \mathbf{0} \tag{5}$$

are obtained where the (n x 1)-flux vectors $\Phi_g = \mathbf{col}\{\phi_{gi}\}$, $\Phi_p = \mathbf{col}\{\phi_{pi}\}$, $\Phi_b = \mathbf{col}\{\phi_{bi}\}$, and $\Phi_r = \mathbf{col}\{\phi_{ri}\}$ correspond to airgaps, poles, backiron, and rotor, respectively; **d** is the identity matrix, and **d**′, **e**, **e**′ are constant geometric distribution matrices as defined in the appendix. The above matrix equations (1) to (5) represent 4n relationships for 4n unknown magnetic flux values $\phi_{(g,p,b,r)i}$ and 4n unknown magnetic field strength values $H_{(g,p,b,r)i}$ within the AMB-actuator network, (i = 1, 2, ...n). In order to solve the system, 4n additional material equations have to be employed.

4 NONLINEAR CONSTITUTIVE MATERIAL EQUATIONS

For airgap path elements in the network the linear material law

$$\mathbf{H}_g = \mathbf{B}_g / \mu_0 \qquad (6)$$

holds, where $\mathbf{B}_g = \mathbf{col}\{B_{gi}\}$ and $\mu_0 = 4\pi E-7$ H/m is the permeability of free space and approximately of air. The magnetization characteristics for the core material of stator and rotor are nonlinear and will be described by the model of (Hodgdon, 1988a, b). The magnetization process is approximated by a first order differential equation of the form

$$\frac{dH}{dB} = \frac{\dot{H}(t)}{\dot{B}(t)} = \alpha \,\mathrm{sign}(\dot{B})[f(B) - H] + g(B) = \frac{1}{\mu(B, H, \mathrm{sign}(\dot{B}))} \qquad (7)$$

where α is a material constant and f(B) and g(B) are empirical functions to be identified from measurement results for a given material. The magnetization gradient $\mu(B, H, \mathrm{sign}\,\dot{B})$ is called the local permeability of the material and depends on the magnetization state (B, H) and the magnetizing direction $\mathrm{sign}\,\dot{B}$ within the B-H-plane, see Fig. 2, for example. The function f(B)

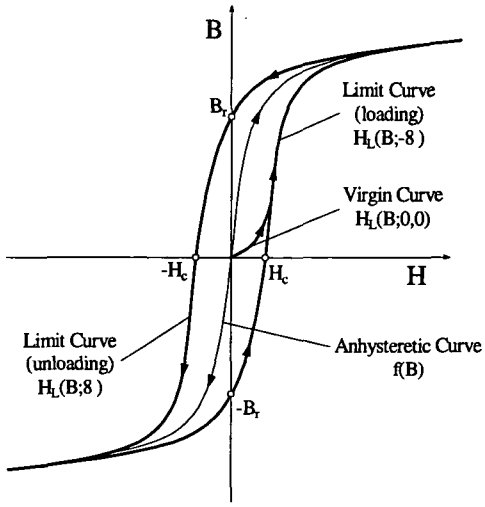

Figure 2. Various magnetizing curves for ferromagnetic materials, after (Hodgdon, 1988a,b) and (Haferl, Springer, 1991).

is called anhysteretic curve. For each network path element of the AMB core material the actual value of the local permeability $\mu(B, H, \mathrm{sign}\,\dot{B})$ is calculated in terms of the magnetization state (B, H) along with the actual magnetizing direction (either loading $\dot{B} > 0$ or unloading $\dot{B} < 0$). The constitutive laws for the core materials of p-, b-, and r-path elements, respectively, can then be written in matrix form

$$\dot{\mathbf{H}}_{p,b,r} = \boldsymbol{\mu}^{-1}{}_{p,b,r}\, \dot{\mathbf{B}}_{p,b,r} \qquad (8)$$

with $\boldsymbol{\mu}_p = \mathbf{diag}[\mu_{pi}]$, $\boldsymbol{\mu}_b = \mathbf{diag}[\mu_{bi}]$, and $\boldsymbol{\mu}_r = \mathbf{diag}[\mu_{ri}]$ being (n x n)-diagonal local permeability matrices for pole, back-iron and rotor material, respectively. It is worth to note that the

material coefficients of the above magnetization model may individually be introduced for different magnetic path elements of the network. Therefore, it is quite simple to consider anisotropic material properties of the stator sheets, for example.

5 ACTUATOR SIMULATION MODEL

Open loop actuator state equations

If the flux densities in the network path elements are considered to be piecewise constant then the flux vectors of the network are given by

$$\boldsymbol{\Phi}_{g,p,b,r} = \mathbf{A}_{g,p,b,r}\,\mathbf{B}_{g,p,b,r} \qquad (9)$$

with $\mathbf{A}_g=\mathbf{diag}[A_{gi}]$, $\mathbf{A}_p=\mathbf{diag}[A_{pi}]$, $\mathbf{A}_b=\mathbf{diag}[A_{bi}]$, and $\mathbf{A}_r=\mathbf{diag}[A_{ri}]$ being (n x n)-diagonal cross section matrices for airgaps, poles, back-iron and rotor path elements, respectively, and $\mathbf{B}_{g,p,b,r}$ being the corresponding (n x 1)-flux density vectors. If fringing effects of the fluxes are neglected and each pole face area is equal to the corresponding constant pole cross section A_p then the airgap flux cross section $A_g \cong A_p$, and from Eqn.(5) and (9) $\mathbf{B}_g \cong \mathbf{B}_p$ holds. Differentiating Eqn.(1), (2) and Eqn.(3), (4) leads to the following system of 3n first order differential equations to determine the flux densities $\mathbf{B}_{p,b,r}$ within the path elements of the core network

$$\begin{aligned}
[\mathbf{e}^T\mathbf{g}(x)\mu_0^{-1}+\mathbf{e}^T\mathbf{p}\boldsymbol{\mu}_p^{-1}]\,\dot{\mathbf{B}}_p + \mathbf{b}\boldsymbol{\mu}_b^{-1}\dot{\mathbf{B}}_b + \mathbf{r}\boldsymbol{\mu}_r^{-1}\dot{\mathbf{B}}_r + \mathbf{e}^T\,[\mathbf{dg}/dt]\mu_0^{-1}\mathbf{B}_p &= \mathbf{e}^T\mathbf{n}\,\dot{\mathbf{I}}\,(t)\\
\mathbf{A}_p\dot{\mathbf{B}}_p \;-\; \mathbf{e}\mathbf{A}_b\,\dot{\mathbf{B}}_b &= \mathbf{0}\\
\mathbf{d}'\mathbf{A}_p\dot{\mathbf{B}}_p \;-\; \mathbf{e}'\mathbf{A}_r\dot{\mathbf{B}}_r &= \mathbf{0}\\
\mathbf{S}^T\mathbf{r}\boldsymbol{\mu}_r^{-1}\dot{\mathbf{B}}_r &= 0 \qquad (10)
\end{aligned}$$

while the corresponding magnetic field strength vectors $\mathbf{H}_{p,b,r}$ can be calculated from integrating Eqn.(8).

The voltage drop vector $\mathbf{U}$ in the coils can be calculated from

$$\mathbf{U} = \mathbf{r}_c\,\mathbf{I} + \mathbf{A}_p\mathbf{n}\,\dot{\mathbf{B}}_p \qquad (11)$$

where $\mathbf{r}_c=\mathbf{diag}[r_{ci}]$ is a (n x n)-diagonal coil resistance matrix. In most cases the coils are supplied by m < n independent current sources $\mathbf{I}_s=\mathbf{col}\{I_{si}\}$ with corresponding supply voltages $\mathbf{U}_s=\mathbf{col}\{U_{si}\}$, i = 1, 2, ...m. Then the relations

$$\mathbf{I} = \mathbf{D}\,\mathbf{I}_s\,, \qquad (12)$$

$$\mathbf{U}_S = \mathbf{D}^T\mathbf{U} \qquad (13)$$

hold, where $\mathbf{D}$ is a so-called (n x m)-current distribution or connection matrix. An example of $\mathbf{D}$ for an (n = 8)-pole AMB with m = 4 independent current sources is shown in the appendix, see also Fig. 3 for this example. From Eqn.(11), (12), (13) the relation

$$\mathbf{U}_S = \mathbf{D}^T\mathbf{r}_c\mathbf{D}\,\mathbf{I}_s + \mathbf{D}^T\mathbf{A}_p\mathbf{n}\,\dot{\mathbf{B}}_p \qquad (14)$$

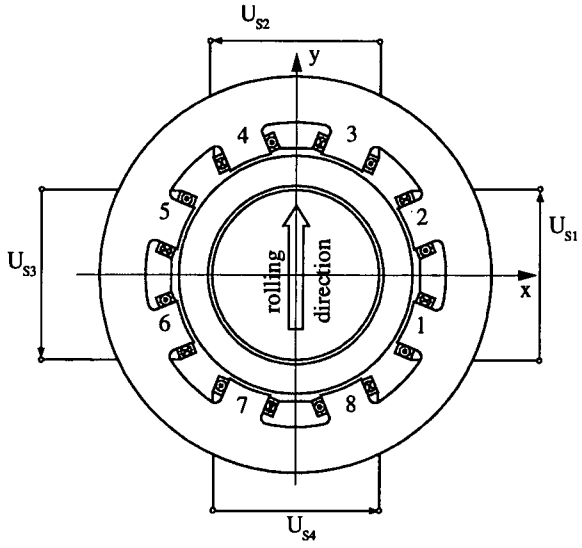

Figure 3. Radial AMB with m=4 coil-supply voltages U_{S1}, U_{S2}, U_{S3}, U_{S4} and pole numbers n = 1 to 8. The arrow indicates the direction of rolling during the manufacturing process of the anisotropic stator sheets.

is obtained. When introducing an actuator state vector **Z** with (6n + m) unknown states

$$\mathbf{Z} = [\mathbf{B_p}^T \mathbf{B_b}^T \mathbf{B_r}^T \mathbf{H_p}^T \mathbf{H_b}^T \mathbf{H_r}^T \mathbf{I_s}^T]^T \quad , \tag{15}$$

Eqn.(8), (10), (14) can be written in the first order compact matrix form

$$\mathbf{R(Z, x)}\,\dot{\mathbf{Z}} + \mathbf{G}(\dot{\mathbf{x}})\mathbf{Z} = \mathbf{U_A}(t) \quad . \tag{16}$$

The system matrices **R(Z,x)**, **G**($\dot{\mathbf{x}}$) and the voltage supply vector $\mathbf{U_A}(t)$ are shown in the appendix. Note, that the above system is nonlinear since the system matrix **R** is not constant but depends on the state **Z** itself. Further, **R** and **G** are time varying with the rotor displacements **x**(t). The field strengths within n airgaps are determined from the vector $\mathbf{H_g} = \mathbf{B_p}/\mu_0$ according to Eqn. (6).

Closed loop rotor-AMB equations

Considered is a horizontal single mass rotor, for example, with mass M and weight Mg. The attractive magnetic force components exerted to the rotor by n poles in x- and y-direction, respectively, are calculated from

$$\mathbf{F_m}(\mathbf{B_p}^2) = \begin{Bmatrix} F_x(\mathbf{B_p}^2) \\ F_y(\mathbf{B_p}^2) \end{Bmatrix} = \frac{1}{2\mu_0} \begin{bmatrix} \mathbf{B_p}^T \mathbf{A_{pc}}\, \mathbf{B_p} \\ \mathbf{B_p}^T \mathbf{A_{ps}}\, \mathbf{B_p} \end{bmatrix}, \tag{17}$$

see Figure 1, with diagonal (n x n)-matrices $\mathbf{A_{pc}} = \mathbf{diag}\,[A_{pi} \cos \alpha_i]$ and $\mathbf{A_{ps}} = \mathbf{diag}\,[A_{pi} \sin \alpha_i]$ to be calculated from the pole attitude angles α_i and the pole face areas A_{pi}, (i = 1, ...n). From

the shaft displacement vector $\mathbf{x} = [x, y]^T$ the air gap lengths matrix as introduced in Eqn.(1) is calculated in a linearized form to

$$\mathbf{g(x)} \doteq \mathbf{g}_0 - x\mathbf{c}_\alpha - y\mathbf{s}_\alpha \qquad (18)$$

with $\mathbf{c}_\alpha = \mathbf{diag}\,[\cos\alpha_i]$, $\mathbf{s}_\alpha = \mathbf{diag}\,[\sin\alpha_i]$ and $\mathbf{g}_0$ being the air gap matrix for the centered shaft position $\mathbf{x} = \mathbf{0}$. In general, $\mathbf{g}_0 = g_0\mathbf{diag}[1,...1]$, i.e., the shaft zero position gap lengths are equal for all poles. If the shaft is displaced by a velocity $\dot{\mathbf{x}}$ the air gap rate of change is given by $[\mathbf{dg}/dt] = -\dot{x}\mathbf{c}_\alpha - \dot{y}\mathbf{s}_\alpha$.

Applying Newton's law to the shaft yields

$$\mathbf{M}\ddot{\mathbf{x}} = \mathbf{F}_m + \mathbf{F}_{ex}(t), \qquad (19)$$

with the mass matrix $\mathbf{M} = \mathbf{diag}[M,M]$. The pole flux densities $\mathbf{B}_p$ can be picked from the actuator state vector $\mathbf{Z}$ of Eqn.(15) by $\mathbf{B}_p = \mathbf{S}_p\,\mathbf{Z}$, with a corresponding n x (6n + m)-selection matrix $\mathbf{S}_p$ composed of zero- and identity-matrices. Therefore, Eqn.(19) with Eqn.(17) can be written as

$$\mathbf{M}\ddot{\mathbf{x}} - \mathbf{F}(\mathbf{Z}^2) = \mathbf{F}_{ex}(t) \qquad (20)$$

with

$$\mathbf{F}(\mathbf{Z}^2) = \frac{1}{2\mu_0}\begin{bmatrix}\mathbf{Z}^T\mathbf{S}_p{}^T\mathbf{A}_{pc}\,\mathbf{S}_p\mathbf{Z} \\ \mathbf{Z}^T\mathbf{S}_p{}^T\mathbf{A}_{ps}\,\mathbf{S}_p\mathbf{Z}\end{bmatrix}. \qquad (21)$$

The (6n + m) x 1-dimensional supply voltage vector $\mathbf{U}_A(t)$ in Eqn.(16) can be determined from a (k x 1)-dimensional control voltage vector $\mathbf{U}_C(t)$ composed of $k \le m$ independent control voltages in the form

$$\mathbf{U}_A(t) = \mathbf{V}\,[\mathbf{U}_C(t) + \mathbf{U}_B] \qquad (22)$$

where $\mathbf{V}$ is a (6n + m) x k-voltage distribution matrix, and $\mathbf{U}_B$ is a constant biasing voltage vector corresponding to a prestressed static state of the rotor bearing system. For a linear rotor output control of the voltage the control law may have the form

$$\mathbf{U}_C = -\mathbf{L}\,\mathbf{x} = -[\mathbf{P} + \mathbf{D1}\,\frac{d\mathbf{x}}{dt} + \mathbf{D2}\,\frac{d^2\mathbf{x}}{dt^2}] \qquad (23)$$

with $\mathbf{L}$ being a linear matrix differential operator, in general. In the above example of Eqn.(23) $\mathbf{L}$ corresponds to a PD2-controller. In this case the closed-loop nonlinear rotor-AMB system becomes the final form

$$\begin{aligned}&\mathbf{M}\ddot{\mathbf{x}} - \mathbf{F}(\mathbf{Z}^2) = \mathbf{F}_{ex}(t) \\ &\mathbf{R}(\mathbf{Z},\mathbf{x})\dot{\mathbf{Z}} + \mathbf{G}(\dot{\mathbf{x}})\mathbf{Z} + \mathbf{V}[\mathbf{P}\mathbf{x} + \mathbf{D1}\,\dot{\mathbf{x}} + \mathbf{D2}\,\ddot{\mathbf{x}}] = \mathbf{V}\mathbf{U}_B\,.\end{aligned} \qquad (24)$$

With chosen initial conditions $\mathbf{Z}(0) = \mathbf{Z}_0$, $\mathbf{x}(0) = \mathbf{x}_0$, $\dot{\mathbf{x}}(0) = \mathbf{v}_0$, 3n flux densities and 3n magnetic field strengths in the core material along with m source currents and 2 shaft

displacements can simultaneously be integrated in the time domain. Note, that the system matrix $\mathbf{R(Z,x)}$ is not constant and therefore, has to be inverted at each time step within the numerical integration of the system Eqn.(24).

6 NUMERICAL EXAMPLE

The simulation model is carried out with MATLAB- and SIMULINK-software packages on a regular 166 MHz-Pentium PC (512 KB Cache, 64 MB RAM). An (n = 8)-pole bearing stator is considered as shown in Fig.3. The (52 x 1)-supply voltage vector $\mathbf{U_A} = [\mathbf{0}^T, \mathbf{0}^T, \mathbf{0}^T, \mathbf{0}^T, \mathbf{0}^T, \mathbf{0}^T, U_1, U_2, U_3, U_4]^T = \mathbf{V}[\mathbf{U_C}(t) + \mathbf{U_B}]$ is composed from $\mathbf{U_C}(t) = [U_x(t), U_y(t), 0]^T$ and $\mathbf{U_B} = [0, 0, U_B]^T$, where U_x, U_y are k = 2 control voltages, respectively, for the horizontal x- and the vertical y-axes of the bearing and U_B is a biasing voltage. The (52x 4)- voltage distribution matrix has the form

$$\mathbf{V} = \left[\begin{array}{c|cccc} & 1 & 0 & -1 & 0 \\ \mathbf{0,0,0,0,0,0} & 0 & 1 & 0 & -1 \\ & 1 & 1 & 1 & 1 \end{array}\right]^T .$$

As usual, the biasing voltage has been chosen such that the static flux density in the poles is about 50 % of the material saturation value B_{max}. In this example, a linear decentralized PD2 controller is introduced according to Eqn.(23) with

$$\mathbf{P} = \begin{bmatrix} P_x & 0 \\ 0 & P_y \\ 0 & 0 \end{bmatrix}, \quad \mathbf{D1} = \begin{bmatrix} D1_x & 0 \\ 0 & D1_y \\ 0 & 0 \end{bmatrix}, \quad \mathbf{D2} = \begin{bmatrix} D2_x & 0 \\ 0 & D2_y \\ 0 & 0 \end{bmatrix}.$$

The controller coefficients $P_{x,y}$, $D1_{x,y}$, $D2_{x,y}$ have been designed by pole placement of the closed loop transfer function of the linearized and decoupled actuator equations at the static centered position of the rotor; for details, see (Schlager, 1997). Some geometric bearing data used for this example are presented in Table I.

TABLE I - BEARING DATA

Stator Sheet Diameters	Rotor Sheet Diameters
d_{out} = 186 mm	d_{out} = 115 mm
d_{inn} = 144 mm	d_{inn} = 84 mm
d_{Pole} = 116 mm	airgap = 0,5 mm
Bearing Length = 47 mm, Pole Angle = 45°, α_1 = -22,5° (Fig.1), Number of Turns of one Coil N= 76, Coil Resistance r_c = 800 mΩ, Pole Face Area A_p = 987 mm^2.	

In this example, the stator material is assumed to possess anisotropic magnetic properties caused by the sheet manufacturing rolling process. In Figure 3 the sheet rolling direction of the stator material is indicated in the x-y reference frame. Three different parameter sets for the ferromagnetic material model according to (Hodgdon, 1988a,b) and Eqn.(8) have been identified in (Schlager, 1997). Parameter set (I) for the rolling direction y in Fig.3 with a flux

density saturation value of B_{max} = 1.9 T, set (II) for a 90°-direction x, perpendicular to the rolling direction y with B_{max} = 1.5 T, and set (III) for the 45°-direction with B_{max} = 1.7 T. The pole leg path elements 1, 2, 5, 6 (see Fig.3) were modeled by the material parameter set (II) and the pole legs 3, 4, 7, 8 by material set (I). The stator back-iron paths (1-2), (5-6) were modelled by material set (I), the back-iron paths (2-3), (4-5), (6-7), (8-1) were modelled by material set (III) and the back-iron paths (3-4), (7-8) were modelled by material set (II). Each material set contains 7 independent parameters; the coefficient α in Eqn.(7) was chosen to α = 10 T^{-1} for all directions.

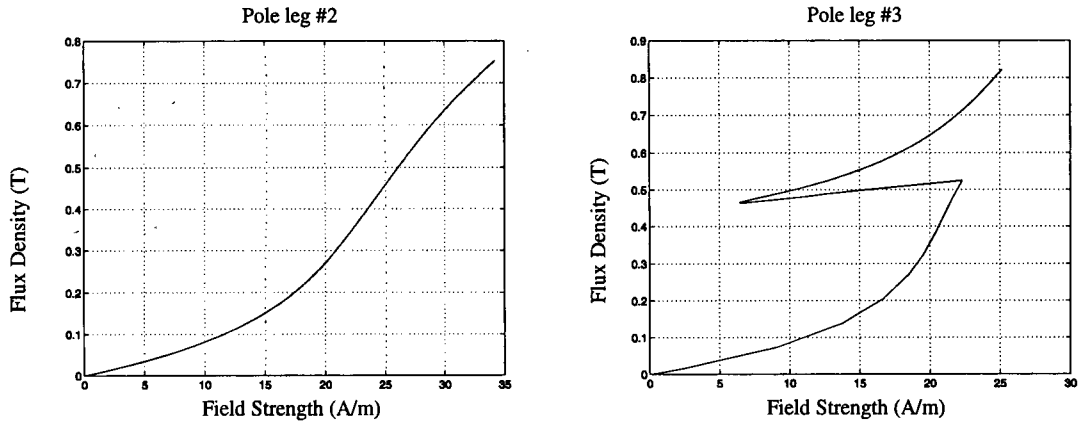

Figure 4. Magnetization trajectories in the pole legs 2 and 3 during rotor lift up operation.

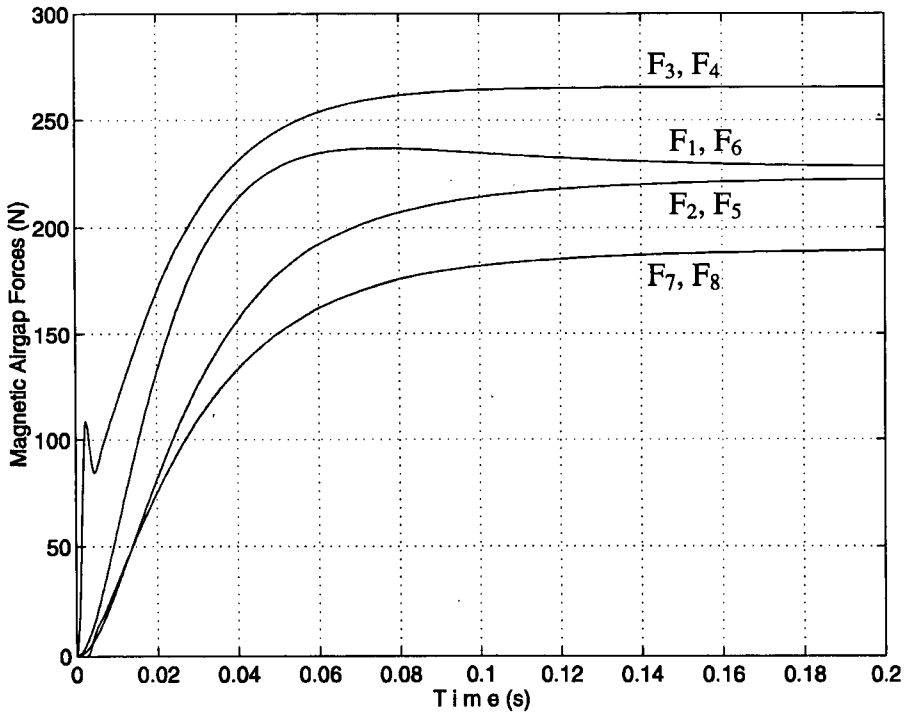

Figure 5. Radial airgap forces F_1 to F_8 during rotor lift up operation.

In a first example, the lift up operation of a 28 kg symmetric rotor in two identical and magnetically anisotropic AMBs is simulated. Because of the loading symmetry the simulation is carried out for one AMB only. At time t = 0 the stationary rotor is at rest in the backup bearings, with an initial radial displacement of -250 μm (= back up bearing clearance), and the voltage is switched on. After about 0.2s the rotor reaches its final position with a vertical offset of 4.1 μm from the center position due to the rotor weight (note that no integral feedback has been introduced in the control law). Fig.4 shows the magnetization trajectories within the pole legs 2 and 3, see Fig.3. A significant hysteresis effect can be observed in the

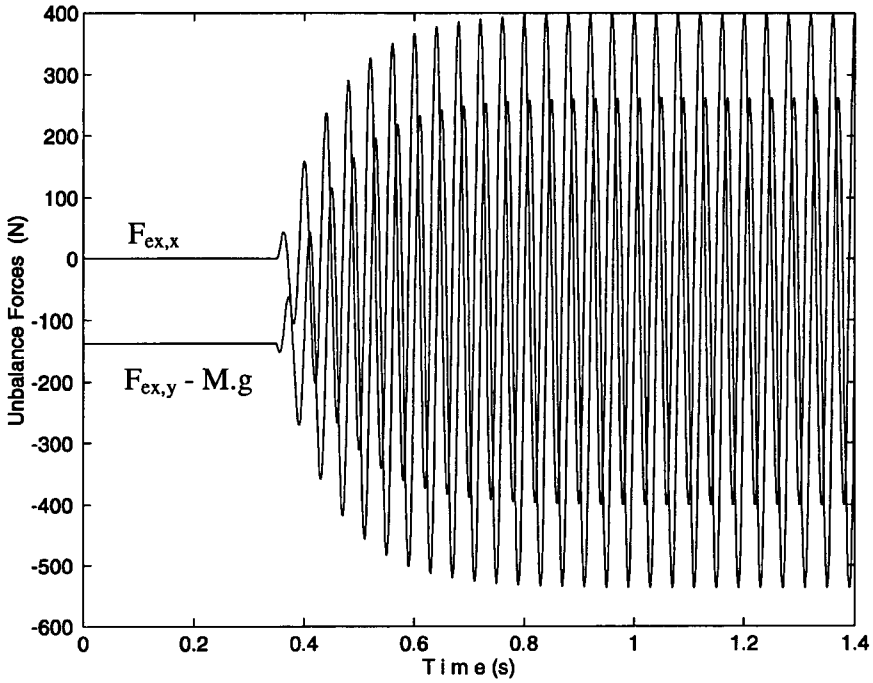

Figure 6. Unbalance excitation forces acting on the rotor after lift up.

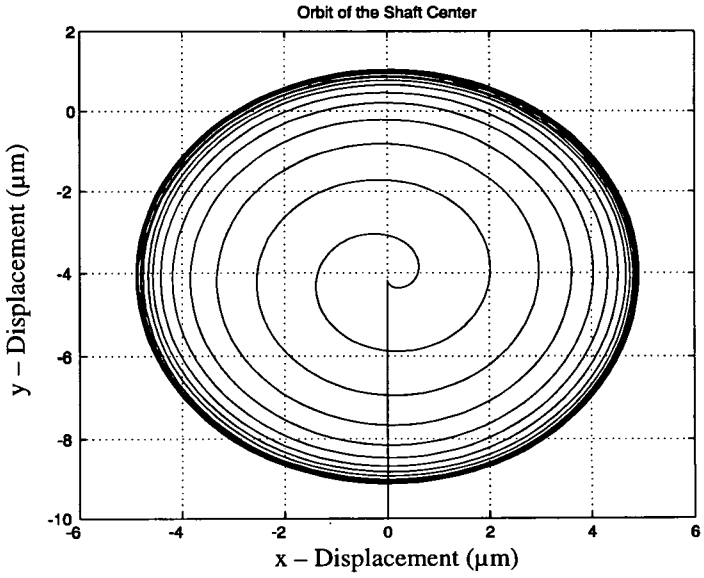

Figure 7. Shaft orbit due to unbalance excitation.

magnetization curve of pole leg 3 caused by an overshoot of the coil supply current I_{S2}. In Fig.5 the build up of the radial magnetic airgap forces during the rotor lift up operation is shown in terms of time. From the y-axis symmetry of the pole arrangement, the material properties and the loading, $F_1 = F_6$, $F_2 = F_5$, $F_3 = F_4$ and $F_7 = F_8$ is obtained. The simulation also shows small back-iron fluxes in the stator paths (8-1) and (2-3) between the pole legs.

In a second example the rotor is exposed to an exponentially growing unbalance excitation force of 400 N amplitude and 25 Hz frequency after the lift up maneuver. Fig.6 shows the time response of the assumed unbalance excitation forces $F_{ex,x}$ and $F_{ex,y}$. In Fig.7 the rotor displacement orbit is shown, starting from the static position of the shaft center. In Fig.8 two magnetization trajectories within the bearing stator material are shown. In the left hand diagram the B-H-curve within the pole leg #3 (see Fig.3) is calculated. After a transient magnetization path a closed loop hysteresis cycle is developed for steady state unbalance vibrations of the rotor. The right hand side diagram shows the magnetization curve within the

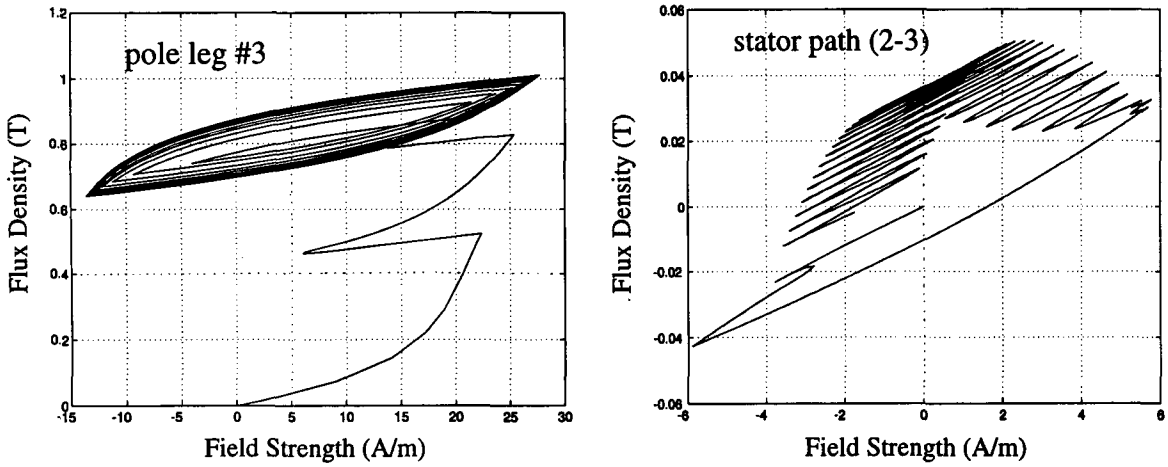

Figure 8. Magnetization trajectories in the stator material due to unbalance excitation.
left: pole leg #3; right: back iron path (2-3), acc. to Fig. 3.

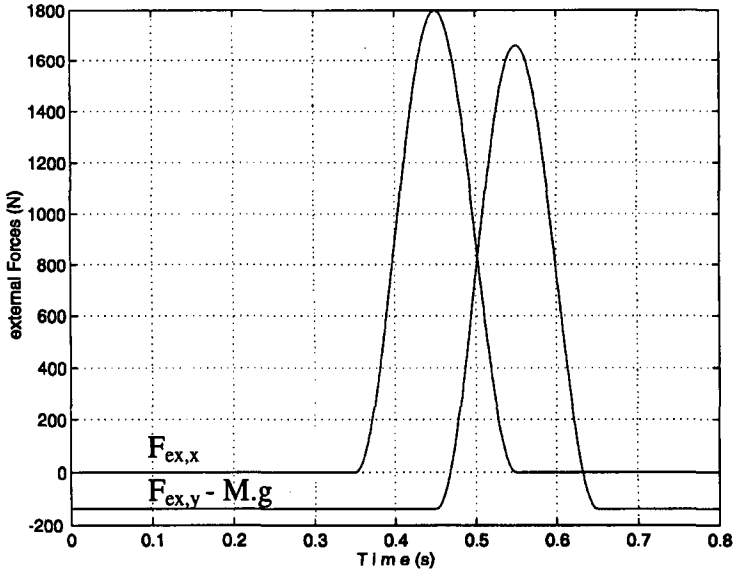

Figure 9. External impact forces applied to the rotor.

back-iron path (2-3) located between poles #2 and #3. Note, that the flux density in the back-iron path is small compared with the pole leg flux density.

In a third example the rotor is exposed to external impact forces $F_{ex,x}(t)$ and $F_{ex,y}(t)$ as shown in Fig.9. Note that the peak forces possess a time offset of 0.1 s. The corresponding rotor displacement trajectory is shown in Fig.10. The full line corresponds to a nonlinear magnetization model the dotted line is calculated from a linear material law of constant permeability without saturation. While the displacement trajectories do not show significant differences this is not true for the magnetization trajectories for poles and stator back-iron paths, as shown in Fig.11. Note that for the above examples no voltage saturation of the amplifieres has been introduced.

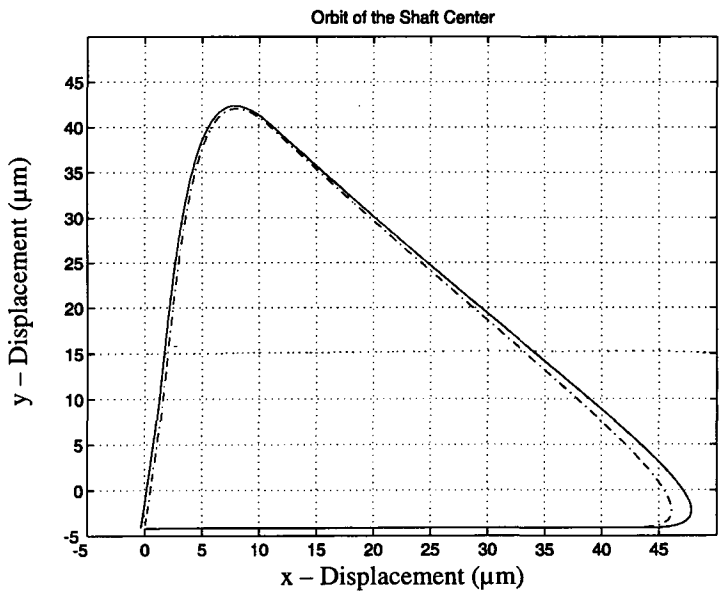

Figure 10. Shaft orbit due external forces, acc. to Fig. 9.
——— nonlinear magnetization model
–·–·–·– linear magnetization model

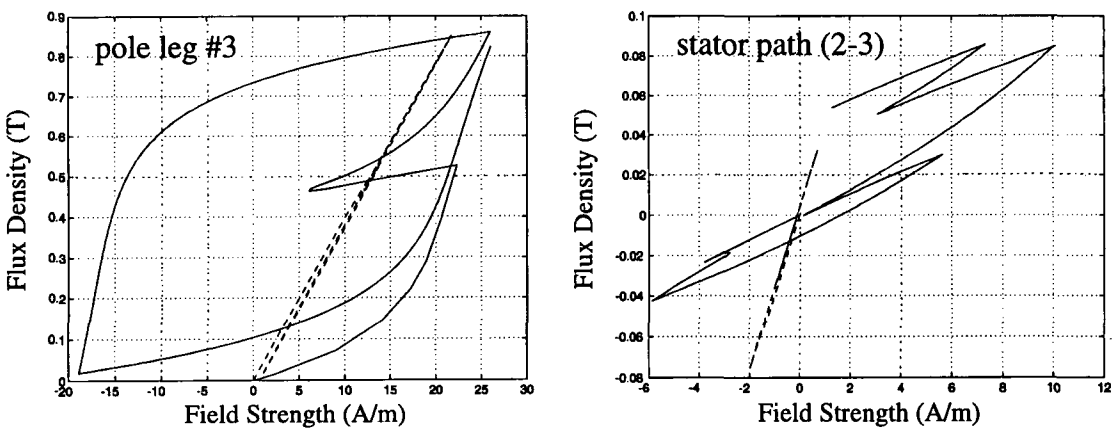

Figure 11. Magnetization trajectories in the stator material.
left: pole leg #3; right: back-iron path (2-3), acc. to Fig. 3.
——— nonlinear magnetization model
-------- linear magentization model

7 CONCLUSION

A magnetic network theory for active magnetic bearing actuators is developed in this paper with which flux densities and field strengths within the stator and rotor materials can be calculated. Nonlinear constitutive magnetization laws are introduced including hysteresis, magnetic saturation and anisotropic stator material properties. An open loop actuator simulation model is formulated in matrix notation with the applied coil control voltages and the shaft motion being input variables and the magnetic actuator state and coil currents being output variables. A closed loop simulation system is obtained by introducing equations of motion for the rotor displacements which are controlled, for example, by a voltage controller.

Three examples are carried out for a radial 8-pole actuator rotor system modelled by 24 network nodes which define 16 ferromagnetic path elements of constant length for the stator, 8 elements for the rotor and 8 variable air gap lengths depending on the rotor displacements. The actuator state vector contains 24 magnetic flux density values, 24 magnetic field strength values and 4 coil current values. A lift up operation of the stationary rotor and a steady state vibration caused by unbalance forces are simulated. Transient vibrations of the rotor are calculated caused by impact forces applied to the rotor, and the difference is shown between linear and nonlinear magnetization characteristics of the core materials. Magnetic back iron fluxes, caused by rolling anisotropy of the stator sheets, are calculated along with steady state hysteresis loops in the pole leg material.

From a series of numerical computations, carried out with the SIMULINK package, it turned out that for very high impact forces exerted to the rotor numerical integration instabilities may occur in the saturation region of Hodgdon's magnetization characteristics. In order to overcome these problems, various integration algorithms have to be tested yet.

ACKNOWLEDGEMENT

The authors gratefully acknowledge the support of this project by the Austrian Science Foundation "Fonds zur Förderung der wissenschaftlichen Forschung (FWF)".

REFERENCES

Haferl, A., Springer, H. 1991. "Simulation von Magnetisierungsprozessen in Magnetlagern-Eine ACSL-Anwendung", Proceedings of 7. Symposium Simulationstechnik (ASIM-Tagung), Hagen (Germany), Verlag Vieweg.

Hodgdon, M.L. 1988a. "Applications of a Theory of Ferromagnetic Hysteresis", IEEE Transactions on Magnetics, Vol.24, No.1.

Hodgdon, M.L. 1988b. "Mathematical Theory and Calculations of Magnetic Hysteresis Curves", IEEE Transactions on Magnetics, Vol.24, No.6.

Maslen, E.H., Meeker, D.C. 1994 "Bias Linearization and Decoupling for Active Magnetic Bearings: A Generalized Theory", Proceedings of the Fourth International Symposium on Magnetic Bearings, Zürich.

Maslen, E.H., Meeker, D.C. 1995. "Fault Tolerance of Magnetic Bearings by Generalized Bias Current Linearization", IEEE Transactions on Magnetics, Vol.31, No.3.

Schlager, G. 1997. "Numerische Simulation von magnetischen Netzwerken in aktiven Magnetlagern", Master Thesis, Department of Mech. Eng., University of Technology, Vienna, Austria.

Schmidt, E., Platter, T., Springer, H. 1996. "Force and Stiffness Calculations in Magnetic Bearings-Comparison Between Finite Element Method and Network Theory", Fifth International Symposium on Magnetic Bearings, Kanazawa (Japan).

Springer, H., Maslen, E.H., Humphris, R.R. 1990. "Nonlinear Hysteresis Effects in Electromagnetic Bearings", Proceeding of Third International Conference on Rotordynamics, Lyon (France).

APPENDIX

Geometric distribution matrices

$$\underset{(n-1)\times n}{\mathbf{d}'} = \begin{bmatrix} 1 & & & & 0 \\ & 1 & & & 0 \\ & & \ddots & & \vdots \\ & & & \ddots & \vdots \\ & & & 1 & 0 \end{bmatrix} \quad \underset{n\times n}{\mathbf{e}} = \begin{bmatrix} 1 & & & & & -1 \\ -1 & 1 & & & & \\ & -1 & \ddots & & & \\ & & \ddots & \ddots & & \\ & & & \ddots & 1 & \\ & & & & -1 & 1 \end{bmatrix} \quad \underset{(n-1)\times n}{\mathbf{e}'} = \begin{bmatrix} 1 & & & & -1 \\ -1 & 1 & & & \\ & -1 & \ddots & & \\ & & \ddots & \ddots & \\ & & & -1 & 1 & 0 \end{bmatrix}$$

Actuator first order system matrix, (6n + m) x (6n + m), depending on the shaft displacements $\mathbf{x} = [x, y]^T$.

$$\mathbf{R}(\mathbf{Z}, \mathbf{x}) = \begin{array}{c|cccccc|c} n & n & n & n & n & n & m & \\ \hline \mathbf{e}^T\mathbf{g}(\mathbf{x})\mu_0^{-1} + \mathbf{e}^T\mathbf{p}\mu_p^{-1} & \mathbf{b}\mu_b^{-1} & \mathbf{r}\mu_r^{-1} & \mathbf{0} & \mathbf{0} & \mathbf{0} & -\mathbf{e}^T\mathbf{n}\mathbf{D} & n \\ \mathbf{A}_p & -\mathbf{e}\mathbf{A}_b & \mathbf{0} & \mathbf{0} & \mathbf{0} & \mathbf{0} & \mathbf{0} & n \\ \mathbf{d}'\mathbf{A}_p & \mathbf{0} & -\mathbf{e}'\mathbf{A}_r & \mathbf{0} & \mathbf{0} & \mathbf{0} & \mathbf{0} & n \\ \mathbf{0} & \mathbf{0} & \mathbf{S}^T\mathbf{r}\mu_r^{-1} & \mathbf{0} & \mathbf{0} & \mathbf{0} & \mathbf{0} & \\ \mathbf{d} & \mathbf{0} & \mathbf{0} & -\mu_p & \mathbf{0} & \mathbf{0} & \mathbf{0} & n \\ \mathbf{0} & \mathbf{d} & \mathbf{0} & \mathbf{0} & -\mu_b & \mathbf{0} & \mathbf{0} & n \\ \mathbf{0} & \mathbf{0} & \mathbf{d} & \mathbf{0} & \mathbf{0} & -\mu_r & \mathbf{0} & n \\ \mathbf{D}^T\mathbf{A}_p\mathbf{n} & \mathbf{0} & \mathbf{0} & \mathbf{0} & \mathbf{0} & \mathbf{0} & \mathbf{0} & m \end{array}$$

Current distribution matrix for an n = 8-pole AMB with m = 4 voltage supplies

$$\mathbf{D} = \begin{bmatrix} -1 & 1 & 0 & 0 & 0 & 0 & 0 & 0 \\ 0 & 0 & 1 & -1 & 0 & 0 & 0 & 0 \\ 0 & 0 & 0 & 0 & -1 & 1 & 0 & 0 \\ 0 & 0 & 0 & 0 & 0 & 0 & 1 & -1 \end{bmatrix}^T$$

Actuator system matrix, (6n + m) x (6n + m), depending on shaft displacement velocity $\dot{\mathbf{x}}$

$\mathbf{G}(\dot{\mathbf{x}}) =$

n	n	n	n	n	n	m	
$\mathbf{e}^T[dg/dt]\mu_o^{-1}$	**0**	**0**	**0**	**0**	**0**	**0**	n
0	**0**	**0**	**0**	**0**	**0**	**0**	n
0	**0**	**0**	**0**	**0**	**0**	**0**	n
0	**0**	**0**	**0**	**0**	**0**	**0**	n
0	**0**	**0**	**0**	**0**	**0**	**0**	n
0	**0**	**0**	**0**	**0**	**0**	**0**	n
0	**0**	**0**	**0**	**0**	**0**	$\mathbf{D}^T\mathbf{r}_c\mathbf{D}$	m

Actuator voltage supply vector, (6n + m) x 1: $\mathbf{U}_A(t) = [0, ...0, \mathbf{U}_s^T(t)]^T$